Biophysical Journal, Volume 97

**Supporting Material**

# Structural changes to monomeric CuZn Superoxide Dismutase caused by the familial Amyotrophic Lateral Sclerosis associated mutation A4V

Tom Schmidlin, Brian Kennedy, and Valerie Daggett

**Table S1: Percentage of time residues are in contact during WT and mutant simulations**

| Residue 1 | Residue 2 | WT | A4V |
|---|---|---|---|
| 4 | 22 | 0.0 ± 0.0 | 64.3 ± 11.5 |
| 27 | 22 | 94.0 ± 9.5 | 40.7 ± 2.1 |
| 27 | 105 | 60.0 ± 25.5 | 7.0 ± 7.9 |
| 28 | 103 | 66.7 ± 28.4 | 5.3 ± 6.1 |
| 28 | 104 | 63.0 ± 26.2 | 4.0 ± 6.9 |
| 28 | 105 | 54.7 ± 28.4 | 4.0 ± 6.9 |
| 47 | 66 | 0.7 ± 1.2 | 53.7 ± 23.4 |
| 47 | 81 | 2.7 ± 2.5 | 60.7 ± 49.2 |
| 48 | 138 | 69.7 ± 31.4 | 0.0 ± 0.0 |
| 63 | 134 | 57.3 ± 33.2 | 0.0 ± 0.0 |
| 63 | 138 | 58.7 ± 32.7 | 0.7 ± 1.2 |
| 66 | 112 | 2.0 ± 3.5 | 59.0 ± 34.7 |
| 79 | 70 | 93.7 ± 7.1 | 23.7 ± 20.3 |
| 79 | 104 | 0.0 ± 0.0 | 73.7 ± 9.2 |
| 80 | 63 | 76.0 ± 29.9 | 21.0 ± 18.7 |
| 80 | 104 | 0.0 ± 0.0 | 65.0 ± 22.6 |
| 82 | 47 | 88.3 ± 20.2 | 33.0 ± 19.1 |
| 82 | 63 | 62.0 ± 46.7 | 2.3 ± 2.3 |
| 84 | 47 | 96.7 ± 4.0 | 19.0 ± 24.6 |
| 84 | 102 | 56.3 ± 49.7 | 0.0 ± 0.0 |
| 86 | 84 | 44.3 ± 25.5 | 96.0 ± 4.4 |
| 102 | 27 | 22.0 ± 23.8 | 78.0 ± 17.0 |
| 103 | 81 | 88.7 ± 15.3 | 28.0 ± 27.8 |
| 104 | 82 | 80.7 ± 9.6 | 7.3 ± 5.0 |
| 112 | 104 | 100.0 ± 0.0 | 38.3 ± 44.3 |
| 112 | 105 | 99.3 ± 1.2 | 42.7 ± 9.0 |
| 120 | 138 | 57.0 ± 24.8 | 0.0 ± 0.0 |
| 120 | 139 | 74.7 ± 29.9 | 0.3 ± 0.6 |
| 123 | 86 | 97.3 ± 3.1 | 31.3 ± 25.1 |
| 139 | 123 | 17.0 ± 26.1 | 86.7 ± 13.8 |

The contact times and standard deviations shown are the average of 3 simulations of each. These contacts are displayed in **Figure 6**.

**Fig. S1. Differences between WT and A4V simulations.** In each case, WT simulations are shown in red and A4V simulations are shown in blue. (A) Cα-RMSD of three WT and A4V simulations shown vs. time. (B) Histogram of Cα-RMSD for three each of WT and A4V simulations taken at 1 ps time points and divided into 0.1Å bins. (C) SASA of three WT and A4V simulations shown vs. time. (D) Histogram of SASA for three each of WT and A4V simulations taken at 1 ps time points and divided into 100Å$^2$ bins. (E) Cα radius of gyration of three WT and A4V simulations shown vs. time. (F) Histogram of radius of gyration for three each of WT and A4V simulations taken at 1 ps time points and divided into 0.05Å bins. (G) CONGENEAL score of three WT and A4V simulations shown vs. time. (H) Histogram of CONGENEAL score for three each of WT and A4V simulations taken at 1 ps time points and divided into bins of .01 dissimilarity score.

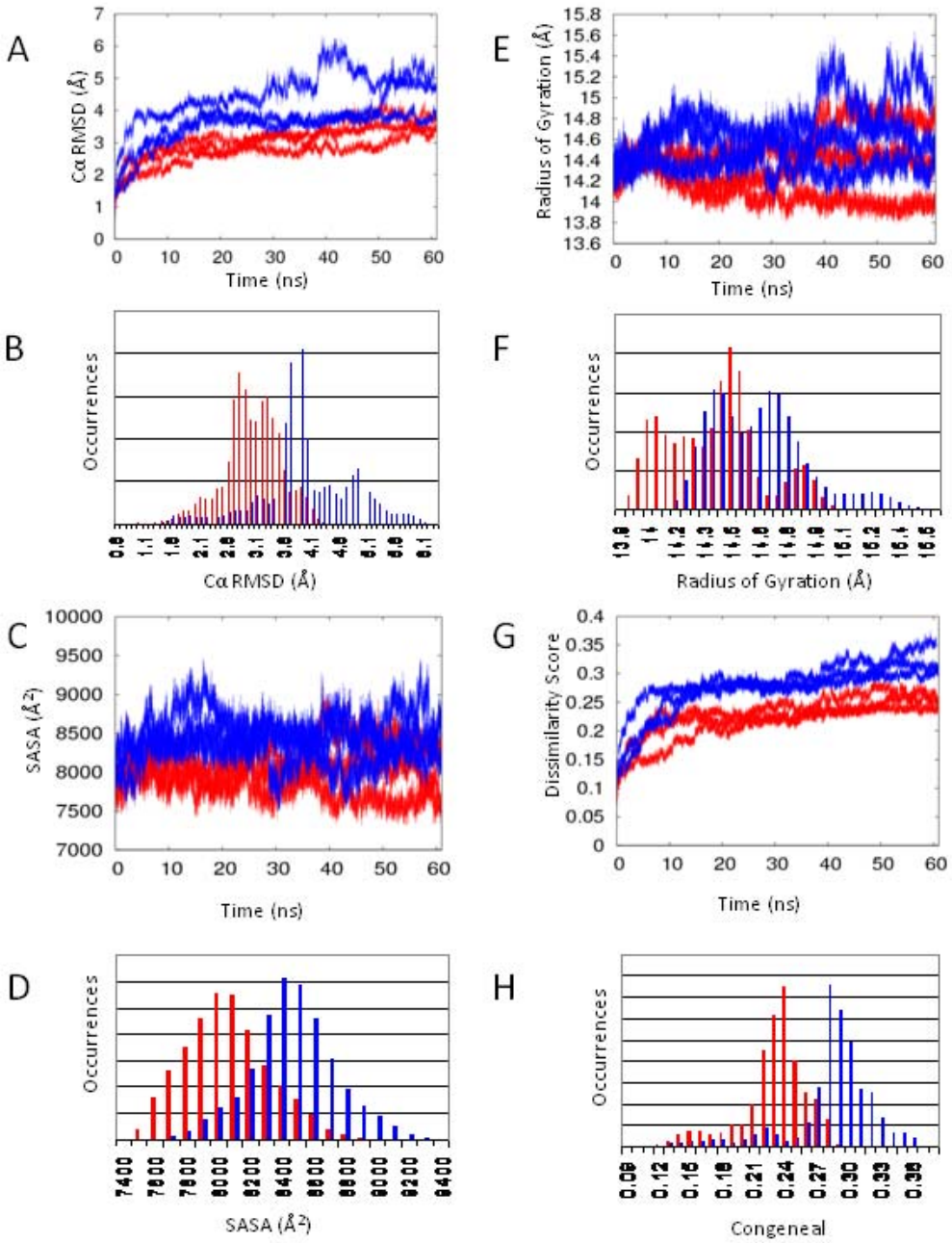

**Fig. S2. Pairwise distances of metal binding atoms.** Pairwise distances of the atoms involved in binding (A) $Cu^{2+}$ and (B) $Zn^{2+}$.

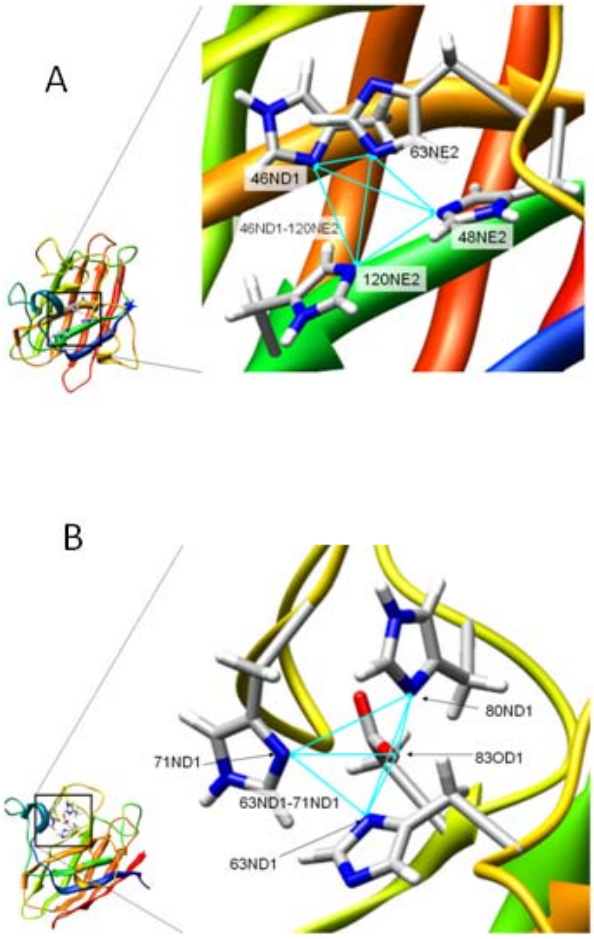

**Fig. S3. Motion of the helix near the $Cu^{2+}$ binding site.** Structures shown are at 5 ns intervals. (A) WT structures. (B) A4V structures, with the final two time points marked to highlight the rotation of the helix in the electrostatic loop.